Preliminary experimental assessment of second-order sliding mode control for wave energy conversion systems

Preliminary experimental assessment of second-order sliding mode control for wave energy conversion systems

Nicolás Faedo[a], Facundo D. Mosquera[b], Carolina A. Evangelista[b], John V. Ringwood[c] and Paul F. Puleston[b]

***Abstract*— Wave energy converters (WECs) inherently necessitate appropriate control technology to operate at optimal efficiency. A particularly well-established family of WEC controllers is based upon a composite structure, where an optimal velocity reference is generated via direct optimal control procedures, followed by a suitable tracking control strategy. Recently, second-order sliding mode (SOSM) control has been shown to be a promising technique for the latter reference tracking problem in WEC systems, being able to achieve robust performance with finite-time convergence. Motivated by the potential of SOSM control within the wave energy field, this paper provides an experimental assessment of SOSM in a tailored hardware-in-the-loop system, located within the facilities of the Centre for Ocean Energy Research, Ireland. We show that the proposed controller is able to achieve robust reference tracking in a variety of wave conditions, consistently maximising energy absorption at virtually the same level of performance obtained in simulation, hence being an ideal candidate for WEC applications.**

I. Introduction

Energy from ocean waves represents a vast untapped resource, with the potential of providing a massive contribution towards global decarbonisation [1]. Though technically feasible, wave energy conversion (WEC) systems have not yet reached a stage of commmercial viability, mostly due to the current elevated levelised cost of energy (LCOE).

It is already well-established that control technology plays a fundamental role in supporting the pathway towards commercialisation of wave energy systems, having the capability to lower the associated LCOE by maximising effective energy extraction from ocean waves [2]. In particular, the family of WEC controllers, often referred as *energy-maximising control* strategies, attempts to optimise the energy conversion efficiency, while guaranteeing safe device operation. A variety of WEC control solutions can be found in the literature, with the vast majority based upon direct optimal control techniques (see *e.g.* [3]). The interested reader is referred to [2], [4] for a comprehensive review of control techniques tailored for the WEC problem.

Recently, a WEC control strategy based upon a combination of so-called moment-based control (see *e.g.* [5], [6]), and second-order sliding modes (SOSM) [7], was presented in [8], with specific application to a nonlinear heaving point absorber WEC system. This technique is defined in terms of a two-level architecture, with an outer loop, featuring a moment-based strategy, which generates an optimal energy-maximising motion trajectory for the specific surrounding wave field. An inner loop then achieves robust finite-time tracking of the corresponding optimal trajectory via a SOSM controller. Though the latter (tracking) technique is shown to be robust with respect to unmodelled WEC dynamics, particularly due to the inherent robustness properties of SOSM, the results presented in [8] are exclusively computed within a simulation environment, *i.e.* there is a lack of experimental assessment of the performance of such a SOSM controller in more 'realistic' scenarios.

Motivated by the potential demonstrated by SOSM to provide robust tracking of optimal motion trajectories for WEC systems, and the intrinsic requirement of real-world testing for its reliable utilisation, we provide, in this paper, an experimental assessment of SOSM within a hardware-in-the-loop (HIL) system, located within the facilities of the Centre for Ocean Energy Research, Ireland. In particular, we assess the performance of the inner tracking SOSM control loop for different sea state (*i.e.* ocean wave) conditions, for a rotational flap-type WEC system. We demonstrate that the SOSM technique is effectively able to provide robust reference tracking, consistently maximising energy absorption at virtually the same level of performance obtained in idealised conditions, *i.e.* in simulation.

The reminder of this paper is organised as follows. Section II describes the experimental HIL system, including a description of the emulated WEC device and associated dynamical model. Section III describes the two-level control architecture, with a focus on design of the reference tracking SOSM technique. Section IV presents the obtained experimental results, offering an appraisal of control performance both in terms of energy-absorption, and effective optimal reference tracking. Finally, Section V summarises the main conclusions of our study.

II. Experimental HIL system

Within this section, we provide a brief description of the HIL system located within the facilities of the Centre for Ocean Energy Research, Maynooth University, Ireland. The testbench is essentially composed of two servo motors (*Panasonic MSME504G1G*), from now on referred to as motor 1 (M1) and motor 2 (M2), respectively, each equipped with an independent driver (*Panasonic MFDHTA464*). M1 and M2 are mechanically coupled accordingly, and the total (resulting) torque is exerted on a flap-like structure, typical

[a]N. Faedo is with the Marine Offshore Renewable Energy Lab, Department of Mechanical and Aerospace Engineering, Politecnico di Torino, Italy (nicolas.faedo@polito.it).

[b] F. D. Mosquera, C. A. Evangelista, and P. F. Puleston are with the Instituto LEICI, Facultad de Ingeniería, Universidad Nacional de La Plata, Buenos Aires, Argentina.

[c]J. V. Ringwood is with the Centre for Ocean Energy Research, Maynooth University, Maynooth, Ireland.

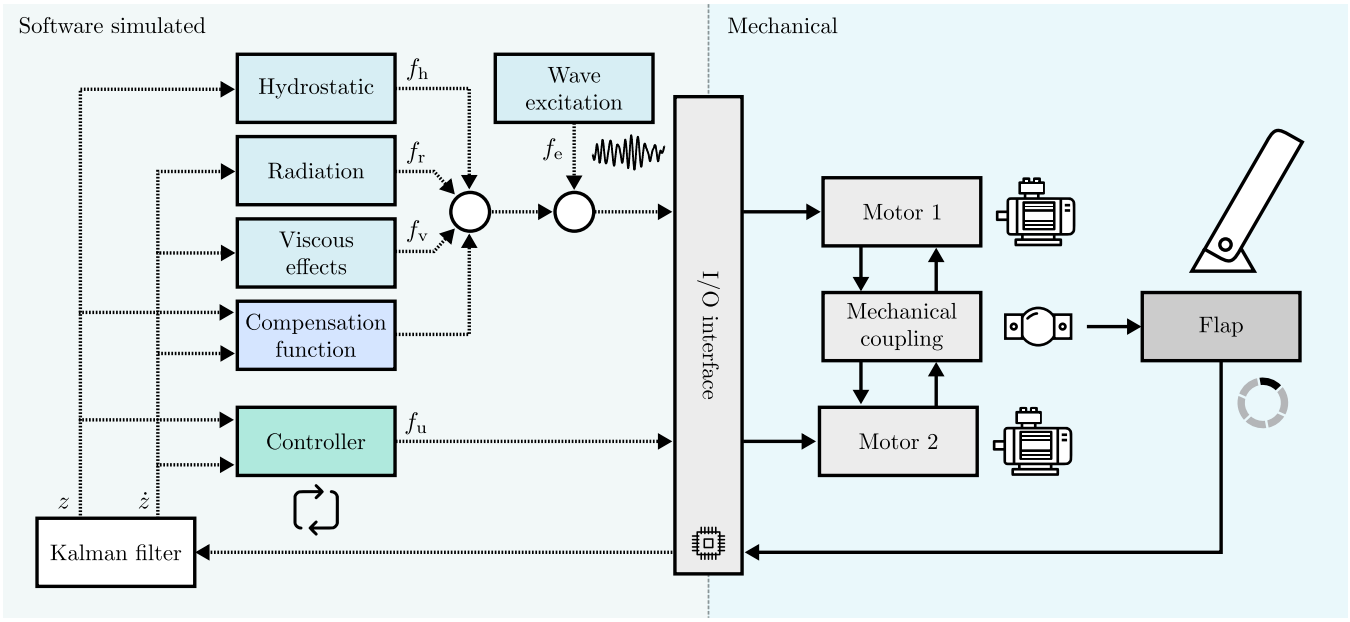

Fig. 1. Schematic representation of the HIL system, identifying software and mechanical parts, accordingly.

of an oscillating wave surge converter (see *e.g.* [9]), mounted below the motors (see Figure 2), which effectively emulates the actual WEC body. The inertia of the flap can be adjusted by including additional weights, according to the specific WEC prototype to be emulated.

In particular, M1 (left-side motor in Figure 2) is used to simulate the hydrodynamics of the WEC device, according to a set of predefined dynamical effects, *i.e.* a user-defined dynamical system. In contrast, M2 (right-side motor in Figure 2) is used as PTO (actuator) system, effectively exerting the requested control torque. Data acquisition is implemented using a rapid prototyping hardware architecture, with any software-emulated component implemented in real-time MATLAB SIMULINK®. The specific input/output (I/O) acquisition board is a *National Instruments PCIe-6343* card.

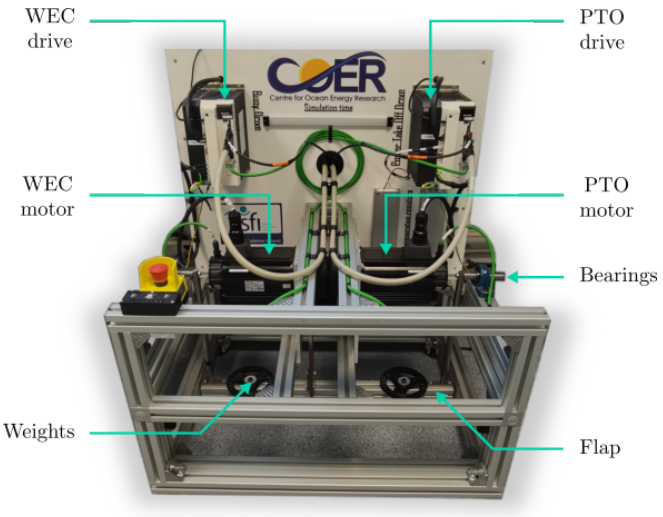

Fig. 2. HIL system considered within this study.

A schematic representation of the HIL functionality is shown in Figure 1, providing clear identification of software and mechanical components, and their respective interactions. Two different 'blocks' can be seen on the software-side, *i.e.* generation of desired hydrodynamic effects, representing the WEC behaviour (see Section II-A), and controller structure, which provides a PTO torque, ideally designed to maximise energy-absorption from the (emulated) wave resource. Both blocks send corresponding torque signals to M1 and M2 via the I/O interface, respectively, which are converted to voltage inputs by each associated driver. An additional block can be seen in Figure 1, termed 'Compensation function', which is responsible for compensating any intrinsic dynamics associated with the HIL rig, *e.g.* damping/stiffness associated with the mechanical design of the flap-like structure, so as to minimise the difference between the desired WEC behaviour, and the actual motion of M1. The angular displacement of the flap structure is measured via an associated encoder, and filtered with a standard Kalman observer, which also provides a corresponding estimate for angular velocity.

A. WEC hydrodynamic model

The device emulated within this study corresponds to a 1/30th scale of an Oyster[1]-like flap WEC system, illustrated schematically in Figure 3. The corresponding full-scale dimensions, referred to Figure 3, are summarised in Table I. The emulated dynamical WEC model is based on linear potential flow theory (see *e.g.* [11]), *i.e.*

$$I_z \ddot{z} = f_\mathrm{h} + f_\mathrm{r} + f_\mathrm{v} + f_\mathrm{e} - f_\mathrm{u}, \tag{1}$$

where $I_z \in \mathbb{R}^+$ denotes the generalised device inertia, $t \mapsto z(t) \in \mathbb{R}$ is the WEC angular displacement, $t \mapsto f_\mathrm{h}(t) \in \mathbb{R}$

[1]The reader is referred to [10] for further detail on the Oyster system.

is the hydrostatic restoring torque, $t \mapsto f_{\mathrm{r}}(t) \in \mathbb{R}$ is the radiation torque (representing the intrinsic fluid memory effects acting on the device), $t \mapsto f_{\mathrm{v}}(t) \in \mathbb{R}$ represents linearised viscous (damping) effects, $t \mapsto f_{\mathrm{e}}(t) \in \mathbb{R}$ is the wave excitation torque, *i.e.* torque exerted on the flap structure by virtue of the wave field, and, finally, $t \mapsto f_{\mathrm{u}}(t) \in \mathbb{R}$ denotes the (PTO) control torque. Note that, as can be appreciated from Figure 3, $\{f_{\mathrm{h}}, f_{\mathrm{r}}, f_{\mathrm{v}}, f_{\mathrm{v}}\}$ are emulated via M1, while f_{u} is exerted independently, via M2.

TABLE I

FULL-SCALE DIMENSIONS OF THE EMULATED WEC SYSTEM.

Parameter	Value
$D1$	2.2 [m]
$D2$	10.0 [m]
$D3$	18.0 [m]
$D4$	8.0 [m]

Though we avoid an explicit derivation for economy of space, we note that equation (1) can be written in terms of an associated strictly proper, continuous-time, minimal, state-space, dynamical system Σ_{W} (see *e.g.* [6]), *i.e.*

$$\Sigma_{\mathrm{W}} : \begin{cases} \dot{\varepsilon} = A\varepsilon + B\left(f_{\mathrm{e}} - f_{\mathrm{u}}\right), \\ y = C\varepsilon, \end{cases} \tag{2}$$

where $\varepsilon(t) \in \mathbb{R}^n$ is the state-vector of Σ_{W}, $y = \dot{z}$ is the output of the WEC system (the flap angular velocity), and the triple $(A, B, C^{\mathsf{T}}) \in \mathbb{R}^{n\times n} \times \mathbb{R}^n \times \mathbb{R}^n$, with $\lambda(A) \subset \mathbb{C}_{<0}$. The relative degree of system (2) with respect to f_{u} is one and, hence, $CB \neq 0$.

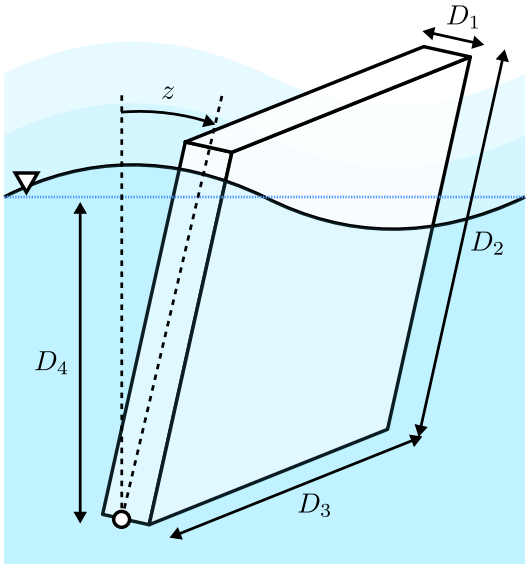

Fig. 3. Schematic representation of the WEC geometry considered.

B. Energy conversion: PTO efficiency

Within this study, the mechanical-to-electrical conversion stage is modelled in terms of an associated PTO efficiency function, as proposed within the benchmark case set by the Wave Energy Control Competition (WEC^{3}OMP) [12] (see also [13]). In particular, let $t \mapsto p_{\mathrm{m}}(t)$ denote the raw absorbed mechanical power, *i.e.*

$$p_{\mathrm{m}} = \dot{z} f_{\mathrm{u}} = y f_{\mathrm{u}}, \tag{3}$$

and let $\eta : \mathbb{R} \to \mathbb{R}$ be the associated PTO efficiency. The absorbed electrical power $t \mapsto p_{\mathrm{e}}(t)$ is hence computed as

$$p_{\mathrm{e}}(p_{\mathrm{m}}) = \eta(p_{\mathrm{m}}) p_{\mathrm{m}}, \tag{4}$$

with the map η defined as

$$\eta(p_{\mathrm{m}}) = \frac{\mu^2 - 1}{2\mu}\mathrm{sign}(p_{\mathrm{m}}) + \frac{\mu^2 + 1}{2\mu}, \tag{5}$$

where $\mu \in [0,\, 1]$ is the so-called efficiency factor, corresponding to the product of the average efficiencies of each emulated PTO stage. Note that the corresponding absorbed electrical power in (4) can be hence computed as

$$p_{\mathrm{e}}(p_{\mathrm{m}}) = \begin{cases} \mu p_{\mathrm{m}} & \text{if } p_{\mathrm{m}} > 0, \\ 0 & \text{if } p_{\mathrm{m}} = 0, \\ p_{\mathrm{m}}/\mu & \text{if } p_{\mathrm{m}} < 0. \end{cases} \tag{6}$$

III. ENERGY-MAXIMISING CONTROL DESIGN

The control design procedure for WEC systems entails an energy-maximising criterion, where the user-supplied control torque f_{u} is designed such that the energy map

$$\mathscr{E} : y f_{\mathrm{u}} \mapsto \int_{\mathcal{T}} p_{\mathrm{e}}(y f_{\mathrm{u}}) \mathrm{d}t, \tag{7}$$

is maximised, for a given time period $\mathcal{T} \subset \mathbb{R}^+$, optimising energy absorption from the wave resource. The design of f_{u}, for the current study, is based on the composite control architecture considered in [8], where an outer control loop provides an optimal energy-maximising (motion) trajectory, which is tracked accordingly by an inner controller (see Figure 4), realised via a SOSM strategy (see Section III-A).

Although, as discussed in Section I, the main concern of our study is the experimental assessment of the inner (tracking) sliding mode controller, we provide, in the following, a brief qualitative description of the outer control loop, which computes an optimal velocity profile according to the current sea-state affecting the WEC system. In particular, this controller adopts a moment-based direct optimal control approach (see *e.g.* [5], [6]): Using the system-theoretic notion of a moment, and its connection to the steady-state output response map of Σ_{W} in (2), the infinite-dimensional optimal control problem

$$\begin{aligned} (P) : &\max_{(y, f_{\mathrm{u}})} \mathscr{E}, \\ &\text{subject to:} \\ &\text{WEC dynamics } \Sigma_{\mathrm{W}}, \varepsilon \in \mathcal{E}, f_{\mathrm{u}} \in \mathcal{U}, \forall t \in \mathcal{T}, \end{aligned} \tag{8}$$

where the sets $\mathcal{E} \subset \mathbb{R}^n$ (closed) and $\mathcal{U} \subset \mathbb{R}$ (compact) represent state and input constraints, respectively, can be discretised (*i.e.* transcribed) into a finie-dimensional Γ-convex nonlinear program (see [5]). Such a parameterisation facilitates efficient numerical computation of an optimal

velocity reference $t \mapsto y^{\mathrm{o}}(t) \in \mathbb{R}$, *i.e.* (approximate) solution of (P), which is fed directly to the inner tracking loop. The interested reader is referred to *e.g.* [5], [6], [14] for a detailed theoretical account of moment-based control, while a corresponding experimental validation of optimal trajectory generation can be found in [15].

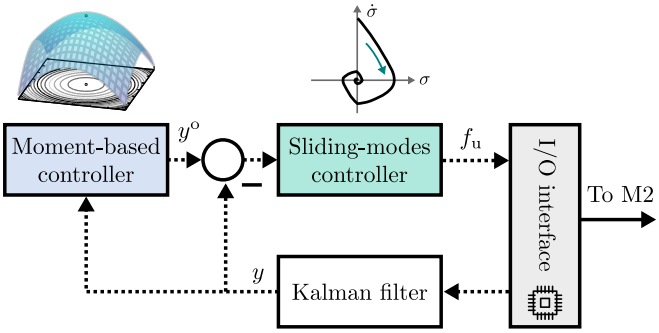

Fig. 4. Schematic illustration of the considered controller structure.

A. Second-order sliding mode

We present, in this section, the specific SOSM algorithm considered within the experimental assessment discussed within this paper, designed to achieve robust tracking of the optimal velocity profile y^{o} provided by the outer (moment-based) control loop (see Section III). In particular, following [8], the sliding variable $\sigma : \mathbb{R}^n \to \mathbb{R}$, $\varepsilon \mapsto \sigma(\varepsilon)$, is defined as

$$\sigma(\varepsilon) = y^{\mathrm{o}} - C\varepsilon, \tag{9}$$

so as to effectively reach the sliding surface $\mathcal{S} : \{\varepsilon \in \mathbb{R}^n : \sigma(\varepsilon) = 0\}$ when $C\varepsilon \to y^{\mathrm{o}}$, which represents, effectively, the maximum energy absorption condition.

Motivated by the fact that the relative degree of system Σ_{W} in (2), with respect to the supplied control torque, is effectively one, a super-twisting (ST) algorithm is adopted for the design of f_{u}. This particular algorithm, which is specifically intended for systems with relative degree one (see *e.g.* [7], [16]), synthesises a continuous control action, contributing to *e.g.* a longer service life of the associated actuator system. Furthermore, the ST control solution does not require an explicit measure of $\dot{\sigma}$, resulting in relative insensitivity to measurement noise. The ST algorithm considered is defined by the following [17] law:

$$f_{\mathrm{u}} = -\alpha_1 |\sigma|^{\frac{1}{2}} \mathrm{sign}(\sigma) - \alpha_2 \int_o^t \mathrm{sign}(\sigma) \mathrm{d}\tau, \tag{10}$$

where $\mathcal{A} = \{\alpha_1, \alpha_2\} \subset \mathbb{R}$ represents the set of ST controller gains. Tuning of the elements in $\mathcal{A}$ typically requires an explicit (closed-form) relation between $\ddot{\sigma}$ and $\dot{f}_{\mathrm{u}}$ in the following structure

$$\ddot{\sigma} = \zeta_{\mathrm{u}}(\varepsilon, f_{\mathrm{u}}) + \zeta_{\dot{\mathrm{u}}}(\varepsilon)\dot{f}_{\mathrm{u}}, \tag{11}$$

where, for the WEC system in (2), the mappings $\zeta_{\mathrm{u}} : \mathbb{R}^n \times \mathbb{R} \to \mathbb{R}$ and $\zeta_{\dot{\mathrm{u}}} : \mathbb{R}^n \to \mathbb{R}$ are

$$\begin{aligned} \zeta_{\mathrm{u}}(\varepsilon, f_{\mathrm{u}}) &= \ddot{y}^{\mathrm{o}} - CB\dot{f}_{\mathrm{e}} - CA^2\varepsilon - CAB\left(f_{\mathrm{e}} - f_{\mathrm{u}}\right), \\ \zeta_{\dot{\mathrm{u}}}(\varepsilon) &\equiv \zeta_{\dot{\mathrm{u}}} = CB. \end{aligned} \tag{12}$$

Finally, assuming that

$$|\zeta_{\mathrm{u}}(\varepsilon, f_{\mathrm{u}})| \leq l_1, \quad l_2 \leq \zeta_{\dot{\mathrm{u}}} \leq l_3, \tag{13}$$

with $\{l_1, l_2, l_3\} \subset \mathbb{R}^+$, sufficient conditions on the elements of the set of ST gains $\mathcal{A}$ for robust finite-time convergence to the sliding manifold $\mathcal{S}$, also intrinsically guaranteeing $\dot{\sigma} = 0$, are [7], [17]

$$\alpha_1 > \frac{\sqrt{2\left(\alpha_2 l_3 + l_1\right)}}{l_2}, \quad \alpha_2 > \frac{l_1}{l_2}. \tag{14}$$

The set $\{l_1, l_2, l_3\}$ in (13) can be computed either by taking into account known potential disturbance/uncertainty bounds of the WEC energy harvesting process, or via numerical/experimental experience.

IV. Experimental results

This section presents the experimental assessment of the energy-maximising control strategy presented in Section III, within the HIL setup described in Section II. In particular, to achieve such an objective, we consider two different operational sea states (SS), described in terms of a stochastic JONSWAP [18] process, with parameters as listed in Table II. The time-traces corresponding to the wave excitation torque f_{e}, for each SS considered, are shown in Figure 6. Note that more than 200 [s] of experiment duration are considered, *i.e.* between $\approx$ 150 and 200 peak periods for SS1 and SS2, respectively, guaranteeing statistically consistent results throughout the assessment presented in this section. In addition, from now on, the efficiency factor μ in (5) is set to $\mu = 0.8$, indicating an 80% of mechanical-to-electrical PTO conversion efficiency.

TABLE II
Considered sea-states for experimental assessment.

	Full-scale		**Scaled (1:30)**	
	H_s	T_p	H_s	T_p
SS1	2.0 [m]	8 [s]	0.066 [m]	1.460 [s]
SS2	2.0 [m]	12 [s]	0.066 [m]	2.191 [s]

The controller gains $\mathcal{A} = \{\alpha_1, \alpha_2\}$, defining the applied control force f_{u} as in (10), are adjusted in-situ, with values set to $\alpha_1 = 14$ and $\alpha_2 = 13$, complying with the condition in (14), where the bounds in (13) are defined as $l_1 = 5$, $l_2 = 0.4$, and $l_3 = 0.8$. Note that these bounds are computed by considering a rather conservative variation in the WEC (HIL) system inertia I_z of $\pm 20\%$ of its nominal value.

Before discussing and assessing the performance of the proposed SOSM controller, Figure 5 presents a 20 [s] time window illustrating both target (ideal WEC motion described via equation (2)), and experimental (HIL motor), velocity outputs, for SS1, with $f_{\mathrm{u}} = 0$, $\forall t$. Note that, while the HIL system is effectively able to reproduce the 'main' desired WEC hydrodynamics, there is, naturally, an inherent error between model and experimental output, due to unmodelled dynamics of the HIL system itself (and hence not 'compensated' correctly - see Section I). Nonetheless, despite this

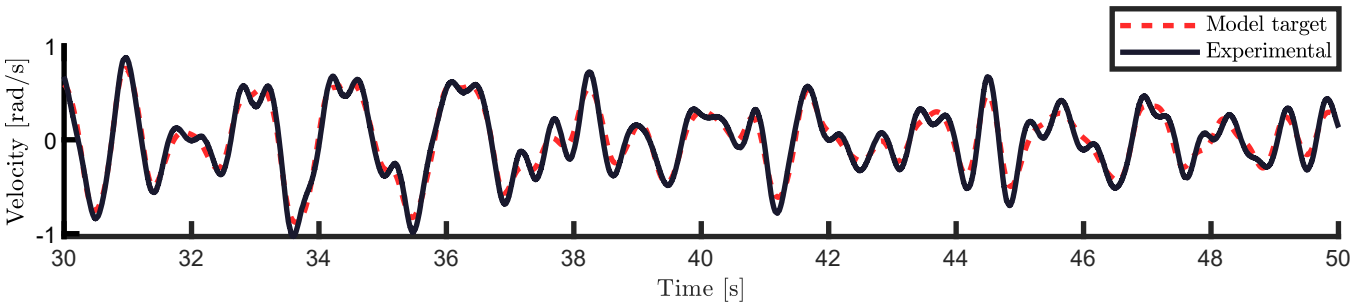

Fig. 5. Target (ideal WEC motion), and experimental (HIL motor), velocity outputs, for SS1, with $f_u = 0$, $\forall t$.

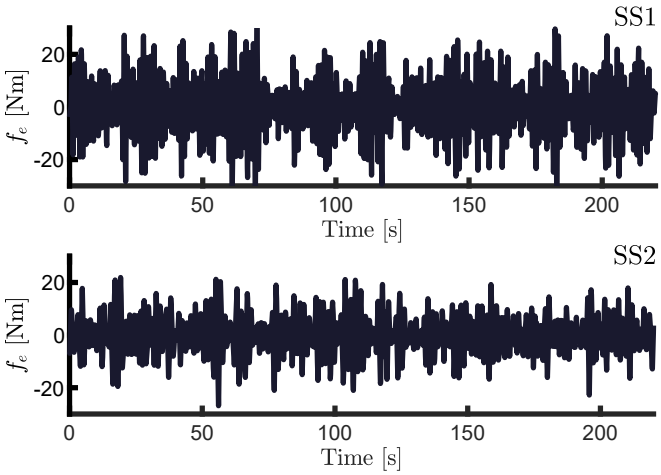

Fig. 6. Wave excitation torque signals f_e for SS1 and SS2.

difference in model and experimental behaviour, we show, throughout this section, that the SOSM is able to achieve satisfactory experimental performance, due to its intrinsic robustness properties.

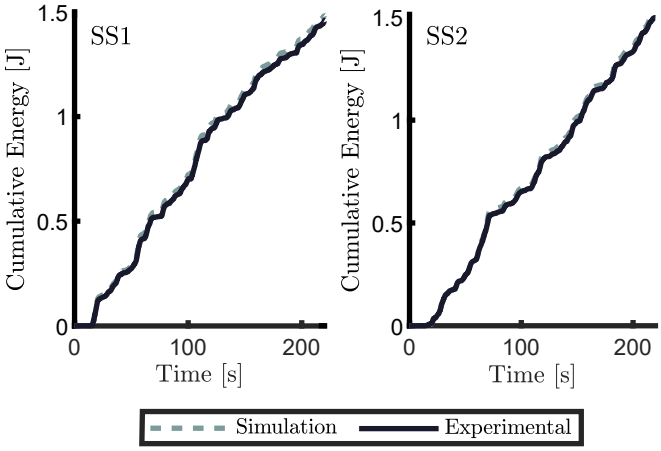

Fig. 7. Cumulative energy for SS1 (left) and SS2 (right), respectively, in both ideal (simulation) and experimental HIL conditions.

We begin the assessment of the SOSM controller by presenting an appraisal of the most relevant performance measure for WEC control techniques, *i.e.* effective energy absorption. In particular, Figure 7 presents cumulative energy for SS1 (left) and SS2 (right), respectively, in both ideal (simulation and control with the exact WEC model defined in (2)), and experimental HIL conditions. It can be readily appreciated that the controller is able to achieve virtually the same amount of ideal energy absorption results in simulation, capturing $\approx 97\%$ of the ideal measure in both scenarios.

The excellent performance obtained in terms of energy absorption is naturally linked to the robust tracking features of the SOSM. We illustrate this fact by analysing the tracking performance of the proposed loop in SS1[2], starting with the results presented in Figure 8. To fully illustrate the behaviour of the SOSM controller, both outer (trajectory generation) and inner (SOSM tracking) loops are left open, *i.e.* the HIL system reproduces the uncontrolled WEC dynamics, until reaching $t = 15$ [s], where the energy-maximising control effectively becomes active. Note that, immediately after the loop is closed, the SOSM is able to drive the WEC velocity towards the optimal reference trajectory y^o with a negligible tracking error, in accordance with the energy performance results presented in Figure 7. A 30 [s] snippet of the corresponding control force, for the SS1 experimental case, can be appreciated in Figure 9.

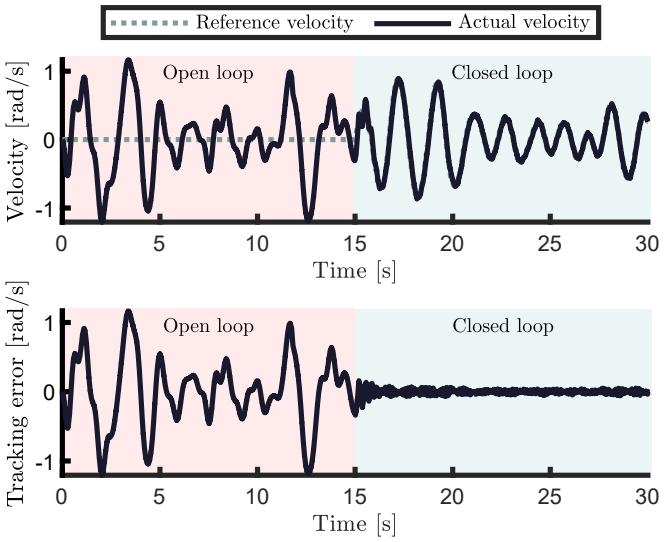

Fig. 8. SOSM tracking performance for SS1. The control loop is closed at $t = 15$ [s].

[2]We avoid presenting tracking performance in SS2 for economy of space (similar results can be shown for SS2, leading to analogous conclusions).

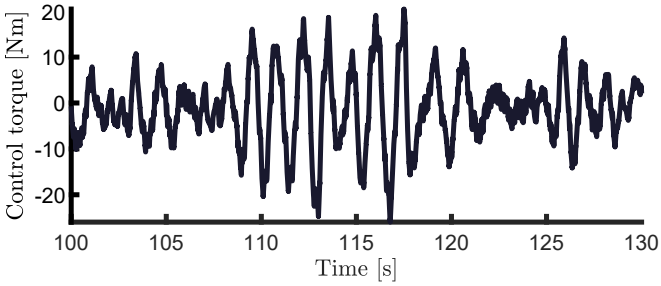

Fig. 9. Snippet (in time) of the corresponding control input for SS1.

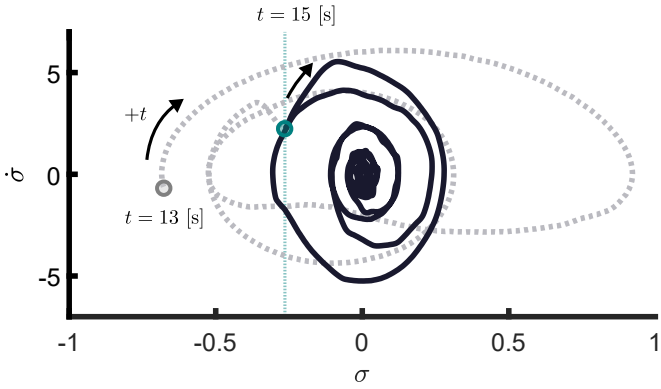

Fig. 10. Experimental σ-$\dot{\sigma}$ phase-plane. The control loop is closed at $t = 15$ [s].

As discussed in Section III-A, when the dynamics of the closed-loop system are governed by the SOSM controller, the trajectories converge to the designed surface in finite-time. To illustrate this, for the WEC experimental assessment case discussed this paper, Figure 10 presents the corresponding trajectories in the σ-$\dot{\sigma}$ phase-plane, for $t \in [13, 20]$ [s]. Note that the dashed line in Figure 10 corresponds to the first 2 [s] (from $t = 13$ [s] to 15 [s]), where the loop is effectively open, *i.e.* the WEC is in uncontrolled conditions. Once the loop is closed, finite-time convergence towards[3] $\sigma = \dot{\sigma} = 0$ can be appreciated, following the characteristic convergence behaviour of the SOSM ST control design.

V. Conclusions

Motivated by the potential demonstrated by SOSM to achieve robust tracking of optimal motion trajectories for WEC systems, this paper presents an experimental validation of SOSM within a HIL testbench, for an Oyster-like flap device. The performance of the controller is assessed for a variety of wave conditions, showing that the SOSM technique is able to consistently maximising energy absorption within 97% of the performance obtained in idealised conditions, *i.e.* in a simulation environment.

Acknowledgment

This project has received funding from the European Union's Horizon 2020 research and innovation programme under the Marie Sklodowska-Curie grant agreement No 101024372. This research was also supported by the Facultad de Ingeniería, Universidad Nacional de La Plata (UNLP), CONICET and Agencia I+D+i, from Argentina.

[3]Note that we refer to *real* sliding as opposed to the *ideal* counterpart, as, in experimental conditions, no approaches can provide an ideal keeping of the prescribed constraint defined by $\mathcal{S}$ (see *e.g.* [7] for further detail).

References

[1] G. Mork, S. Barstow, A. Kabuth, and M. T. Pontes, "Assessing the global wave energy potential," in *International Conference on Offshore Mechanics and Arctic Engineering*, vol. 49118, 2010, pp. 447–454.

[2] J. Ringwood, G. Bacelli, and F. Fusco, "Energy-maximizing control of wave-energy converters: The development of control system technology to optimize their operation," *IEEE Control Systems*, vol. 34, no. 5, pp. 30–55, 2014.

[3] N. Faedo, S. Olaya, and J. V. Ringwood, "Optimal control, mpc and mpc-like algorithms for wave energy systems: An overview," *IFAC Journal of Systems and Control*, vol. 1, pp. 37–56, 2017.

[4] J. V. Ringwood, "Wave energy control: status and perspectives 2020," *IFAC-PapersOnLine*, vol. 53, no. 2, pp. 12 271–12 282, 2020.

[5] N. Faedo, G. Scarciotti, A. Astolfi, and J. V. Ringwood, "Nonlinear energy-maximizing optimal control of wave energy systems: A moment-based approach," *IEEE Transactions on Control Systems Technology*, vol. 29(6), pp. 2533–2547, 2021.

[6] N. Faedo, G. Giorgi, J. V. Ringwood, and G. Mattiazzo, "Optimal control of wave energy systems considering nonlinear froude–krylov effects: control-oriented modelling and moment-based control," *Nonlinear Dynamics*, pp. 1–28, 2022.

[7] L. Fridman, A. Levant *et al.*, "Higher order sliding modes," *Sliding mode control in engineering*, vol. 11, pp. 53–102, 2002.

[8] F. Mosquera, N. Faedo, C. A. Evangelista, P. F. Puleston, and J. V. Ringwood, "Energy-maximising tracking control for a nonlinear heaving point absorber system commanded by second order sliding modes," in *14th IFAC Conference on Control Applications in Marine Systems, Robotics and Vehicles (IFAC CAMS), Lyngby, Denmark (accepted)*, 2022.

[9] T. Whittaker and M. Folley, "Nearshore oscillating wave surge converters and the development of oyster," *Philosophical Transactions of the Royal Society A: Mathematical, Physical and Engineering Sciences*, vol. 370, no. 1959, pp. 345–364, 2012.

[10] A. J. Henry, "The hydrodynamics of small seabed mounted bottom hinged wave energy conerverters in shallow water," Ph.D. dissertation, Queen's University Belfast, 2009.

[11] U. A. Korde and J. V. Ringwood, *Hydrodynamic control of wave energy devices*. Cambridge University Press, 2016.

[12] J. Ringwood, F. Ferri, N. Tom, K. Ruehl, N. Faedo, G. Bacelli, Y.-H. Yu, and R. G. Coe, "The wave energy converter control competition: Overview," in *International Conference on Offshore Mechanics and Arctic Engineering*, vol. 58899. American Society of Mechanical Engineers, 2019, p. V010T09A035.

[13] N. Faedo, G. Giorgi, G. Mattiazzo, and J. V. Ringwood, "Nonlinear moment-based optimal control of wave energy converters with non-ideal power take-off systems," in *ASME 2022 41st International Conference on Ocean, Offshore and Arctic Engineering (OMAE2022), Hamburg, Germany*, 2022.

[14] N. Faedo, G. Scarciotti, A. Astolfi, and J. V. Ringwood, "On the approximation of moments for nonlinear systems," *IEEE Transactions on Automatic Control*, vol. 66(11), pp. 5538–5545, 2021.

[15] N. Faedo, Y. Peña-Sanchez, D. Garcia-Violini, F. Ferri, G. Mattiazzo, and J. V. Ringwood, "Experimental assessment and validation of energy-maximising moment-based optimal control for a prototype wave energy converter," *Control Engineering Practice (under review)*, 2022.

[16] J. Y. Hung, W. Gao, and J. C. Hung, "Variable structure control: A survey," *IEEE transactions on industrial electronics*, vol. 40, no. 1, pp. 2–22, 1993.

[17] A. Levant, "Sliding order and sliding accuracy in sliding mode control," *International journal of control*, vol. 58, no. 6, pp. 1247–1263, 1993.

[18] K. F. Hasselmann, T. P. Barnett, E. Bouws, H. Carlson, D. E. Cartwright, K. Eake, J. Euring, A. Gicnapp, D. Hasselmann, P. Kruseman *et al.*, "Measurements of wind-wave growth and swell decay during the joint north sea wave project (jonswap)." *Ergaenzungsheft zur Deutschen Hydrographischen Zeitschrift, Reihe A*, 1973.